*https://jurnaleeccis.ub.ac.id/* *Jurnal EECCIS Vol. 17, No. 2, Agustus 2023*
p-*ISSN : 1978-3345, e-ISSN(Online): 2460-8122* *pp 66-71*

# Advancing Fault Diagnosis for Parallel Misalignment Detection in Induction Motors Based on Convolutional Neural Networks

Hanif Adi Rahmawan[1], Bambang Lelono Widjianto[2], and Katherine Indrawati[2], Rizki Mendung Ariefianto[3]
[1]Department of Electrical Engineering, Institut Teknologi Sepuluh Nopember, Surabaya, Indonesia
[2]Department of Physics Engineering, Institut Teknologi Sepuluh Nopember, Surabaya, Indonesia
[3]Department of Electrical Engineering, Universitas Brawijaya, Malang, Indonesia
Email: ahwanhanif01@gmail.com, blelono@its.ac.id, katherin@ep.its.ac.id, rizki.mendung.a@ub.ac.id

***Abstract*— Maintenance of machines is highly necessary to prolong the operational lifespan of induction motors. Prioritizing preventive measures is crucial in order to prevent more significant damage to the machinery. One of these measures includes detecting abnormalities, such as misalignment, in the motor shaft. This research is aimed to detect the misalignment of induction motor experimentally by varying the coupling between normal and parallel misalignment. The signal readings were analyzed in the frequency domain using Fast Fourier Transform (FFT). The results revealed that in the case of coupling misalignment, a peak appeared at *f* = 13.5 Hz, whereas in the parallel misalignment condition with a 1 cm misalignment, a peak was found at f+fr = 20 Hz. By utilizing the Convolutional Neural Network (CNN) system, normal and parallel conditions can be detected with an accuracy level of 87.5%.**

***Index Terms*— Induction motor, misalignment, FFT, CNN.**

## I. INTRODUCTION

Electric motors are electromechanical devices that convert electrical energy into mechanical energy. The most widely used electric motor is the induction motor, which is an essential component in many commercially available industrial equipment and processes [1]. This machine is chosen due to its numerous advantages, including being cost-effective, dependable, easy to operate, brushless, not requiring DC excitation, and having a prolonged lifespan without significant issues [2]–[4]. However, despite their reliability, these electromechanical devices are susceptible to various types of faults. Such faults can be destructive, hazardous, lead to production downtime, and cause personal injuries. Therefore, it is crucial to detect these faults as early as possible to prevent total machine failure and unexpected production costs [5], [6].

One of the common faults that can occur in induction motors is misalignment [7]. This problem is the second most common mechanical fault in induction machines after imbalance. It is responsible for more than 70% of rotating machinery vibration problems [8]. Broadly, there are three common types of misalignment such as angular misalignment, parallel misalignment, and a combination of both. In practice, nearly all misalignment conditions observed in motor drive systems are combinations of these two basic types [9].

Special for parallel misalignment, this fault occurs when the rotational axes of the motor and the driven load deviate from being perfectly aligned in parallel, resulting in detrimental effects such as increased mechanical stress, elevated energy consumption, and reduced motor lifespan [10]. To address this issue, proper alignment of rotating machinery is essential to ensure all sensitive components caused misalignment errors can operate within acceptable design limits. Accurate alignment allows for the reduction of axial and radial forces, thereby extending the machine's lifespan while maintaining rotor stability under dynamic operating conditions.

Previous research in [11] conducted experiments and numerical simulations, and the results showed that misalignment generates sidebands in the stator current at frequencies of f+2fr and f-2fr. Another study by [12] utilized Motor Current Signature Analysis (MCSA) to identify radial and angular misalignment when connecting an induction motor to a load through a flexible coupling. In [13], parallel misalignment is analyzed based on stator current, vibration and stray flux. This research used Multilayer Perceptron (MLP) based machine learning algorithm which shows an excellent performance to detect the parallel misalignment fault.

In recent years, Convolutional Neural Networks (CNN) have exhibited outstanding performance in various image recognition and classification tasks [14]. CNN, a class of deep learning algorithms, possess the ability to automatically learn and extract meaningful features from input data, making them well-suited for identifying patterns and abnormalities within motor systems [15], [16]. Leveraging the capabilities of CNN, researchers have begun exploring their potential in detecting misalignment within induction motors.

Therefore, this study aims to propose an innovative detection system that utilizes the CNN method to identify and quantify parallel misalignment in induction motors. Moreover, this study employs MCSA as a method to analyze the frequency spectrum in parallel misalignment in induction motors, with signal processing conducted using Fast Fourier Transform (FFT). The proposed system aims to streamline the misalignment detection process, enabling automated and real-time monitoring and diagnosis. By analyzing the current waveform signals captured by a dedicated sensor, the proposed system can accurately determine the degree of parallel misalignment present in the motor.

## II. METHOD

In this section, the research flow of designing a parallel misalignment detection system on an induction motor based on CNN is outlined, as depicted in Fig. 1.

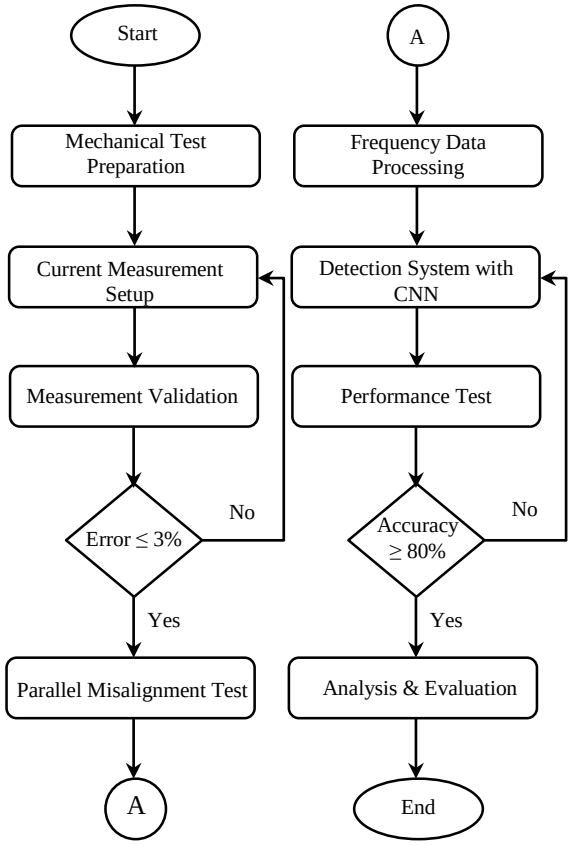


Fig. 1. Flowchart of metodology

### A. *Mechanical Test Preparation*

Experimental testing was carried out by designing a mechanical system comprising an induction motor, machine base, shaft, bearings, load, and coupling as designed in Fig. 2. The induction motor used in this study had specifications of a three-phase induction motor with a voltage of 220/380 V and a power of 0.37 kW. The coupling used was independently fabricated and specifically designed for the parallel misalignment scheme. The experimental procedure began with connecting the induction motor to a three-phase power source on the input side and connecting it to an inverter, which primarily functioned to regulate the speed (rpm) of the induction motor.

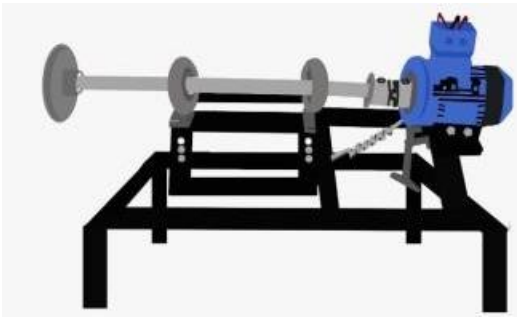

Fig. 2. Mechanical test design

### B. *Current Measurement Setup*

This setup part is developed to measure the stator current of a three-phase induction motor. The current readings are acquired using an SCT 013-000 sensor along with auxiliary components, interconnected to an Arduino Uno microcontroller. The current range sensed by the SCT 013-000 sensor is specified to span from 0 to 100 A. To facilitate data collection, the sensor's current reading range requires reduction to enhance measurement accuracy. Consequently, the SCT current sensor is supplemented with a supportive circuit. This auxiliary circuit serves as an amplifier to convert the current signal into voltage, making it readable by the microcontroller.

The auxiliary circuit components comprise $R_1$ with a value of 10 kΩ, $R_2$ with a value of 10 kΩ, $R_3$ with a value of 680 kΩ, and $C_1$ = 10 µF/16V. The reistance $R_3$ serves as a load resistor, generating varying voltages for ADC microcontroller reading. The resistance value of $R_3$ is set to enable reading currents below 10A. The voltage across the load resistor at peak current must be half of Arduino's reference voltage ($V_{ref}/2$), which is a half of 5V. Subsequently, the primary current value needs calculation using the formula of (1) and (2), which $N$ denoted the SCT turns.

$$I_{prim} = N \times I_{sec} \tag{1}$$

$$I_{prim} = N \times \frac{V_{ref}/2}{R_3} \tag{2}$$

$$I_{prim} = 2000 \times \frac{5/2}{680} = 7.4 \text{ A} \tag{3}$$

The primary current obtained from the auxiliary circuit is 7.4 A, which suffices for current sensor readings. This is occurred due to the motor's induction specifications, where the maximum current generated is 2 A. Furthermore, it is conducted the calibration process through a comparison between the readings from the SCT sensor and the current measured from the ammeter. Data collection on the ammeter spanned 30 seconds, whilst the SCT sensor readings were recorded over a 10-second interval, resulting in a dataset of 2210 data points. This calibration procedure encompassed diverse RPM speed variations on the induction motor.

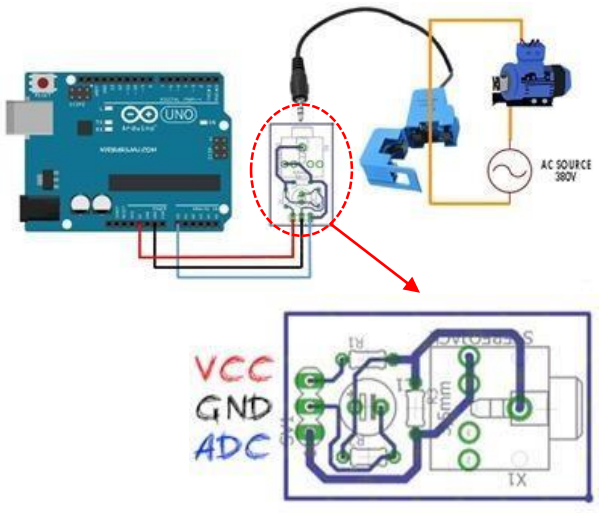


Fig. 3. Current measurement setup and circuit modul

### *C. Paralel Misalignment Test*

In this experiment, two conditions were tested: the first condition being normal or unlignment, and the second being parallel misalignment. Within the parallel condition as shown in Fig. 4, two variations were executed, consisting of 1 cm and 2 cm of parallel misalignment. The induction motor was set to a speed of 400 RPM. Data collection was carried out for 10 seconds over a span of 20 minutes. The effect of misalignment angles on the coupling between the motor and the load shaft was examined through an analysis of the stator current spectra acquired from the experiment. The current spectrum indicated peaks around the fundamental component, as described by (4):

$$f + nf_r \tag{4}$$

where $f$ is frequency, $n$ is a constant, and $f_r$ is angular speed in Hz. The value of $f$ for each normal and parallel data collection differed due to adjustments based on the motor's speed conditions. In the normal condition, $f$ was 13.5 Hz. As for $f_r$, it was derived from the motor speed set by the inverter, which was 400 RPM divided by 60, yielding an $f_r$ value of 6.6 Hz.

### *D. Signal Processing*

The signal processing depicted in Fig. 5 commences with the detection of stator current generated by the induction motor through the SCT sensor. The result of this detection is then converted into analog-to-digital (ADC) format to be utilized as input for the Arduino Uno. The sinusoidal signal obtained from the Arduino Uno's sensor reading is subjected to the Fast Fourier Transform (FFT) to unveil peak amplitude-frequency values. These values are subsequently used to compute misalignment detection predictions using CNN.

During the CNN-based detection process using the normalized FFT signal, several stages are encompassed, which include:

a. Preprocessing: In this stage, the FFT output is normalized to values ranging between 0 and 1.
b. Random Sampling: In this part, a total of 240 data points (120 normal and 120 parallel) are divided, with a composition of 77%, that is, 160 data points for training and 33%, which accounts for 80 data points, designated for testing.
c. CNN: This phase produces a training model for subsequent testing.
d. Testing: In this step, 80 testing data points are processed to generate predictions for parallel misalignment.

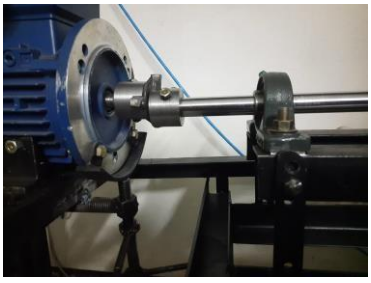

Fig. 4. Parallel misalignment configuration

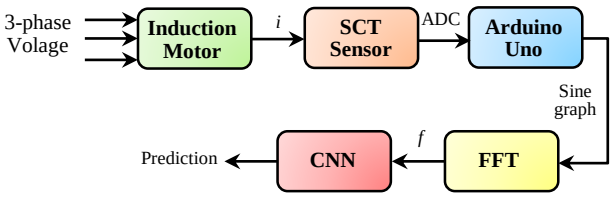


Fig. 5. Block diagram of signal processing

## III. Result and Analysis

### *A. Sensor Calibration Result*

Sensor calibration was carried out by comparing the sensor readings on Arduino with the readings on the ammeter at different RPM variations. Unfortunately, the readings by current sensor were not satisfied with the ammeter readings as shown in Fig. 6. Hence, regression method is applied to obtain a good deal result. The output from this process will be an input for Arduino programming. The regression formula from previous data as given:

$$y = 0.4133x + 1.273 \tag{1}$$

The new data of current measurement after applying regression method is shown in Fig. 7. It is calculated that the standard deviation in the validation measurement of the current sensor (SCT readings) is 0.0521, the uncertainty is about of 0.0197, and the reading error is around 1.22%. Therefore, the reading accuracy of the current sensor is found to be under 3%, indicating a commendable precision in the data readings.

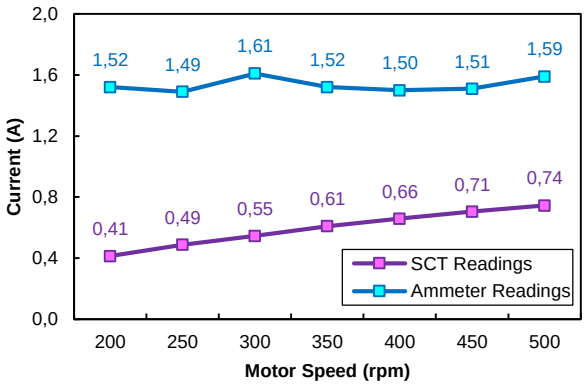


Fig. 6. Measurement result of current between SCT and ammeter

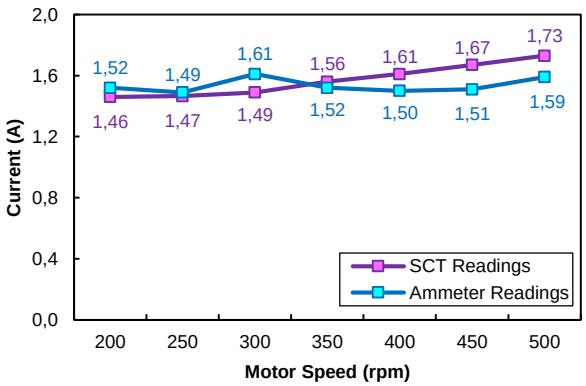


Fig. 7. Measurement result of current between SCT and ammeter

### *B. Signal Processing Result*

In signal processing, a frequency sampling length of 258 data points was employed, collected over a period of 10 seconds. This signal processing was conducted at an induction motor speed of 400 RPM. The results of this signal processing, manifested as sinusoidal current readings across the time domain, are illustrated in Fig. 8a for the normal coupling condition, Fig. 8b for a 1 cm parallel misalignment variation, and Fig. 8c for a 2 cm parallel misalignment variation. It is obvious that notable differences exist among these three conditions. The normal coupling condition demonstrates a more consistent current response in contrast to both the 1 cm and 2 cm parallel misalignment variations.

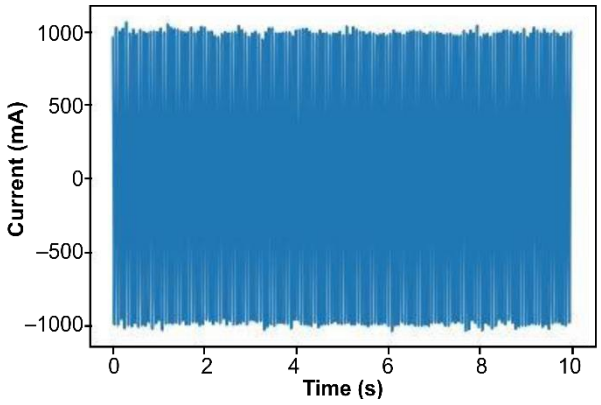


(a)

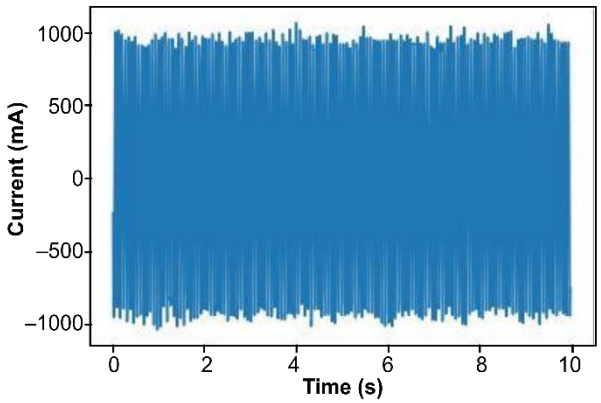


(b)

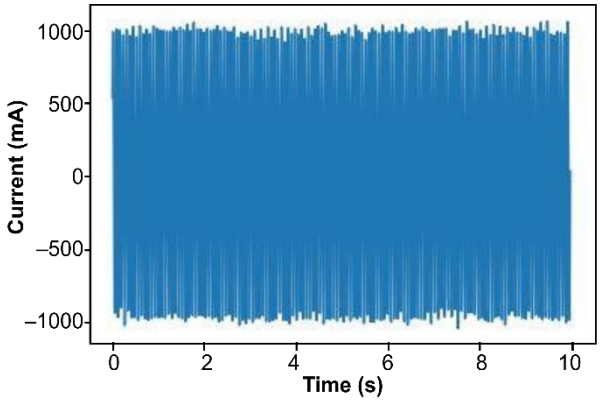


(c)

Fig. 8. Time domain signal of coupling condition: (a) normal (b) 1 cm-parallel misalignment (c) 2 cm-parallel misalignment

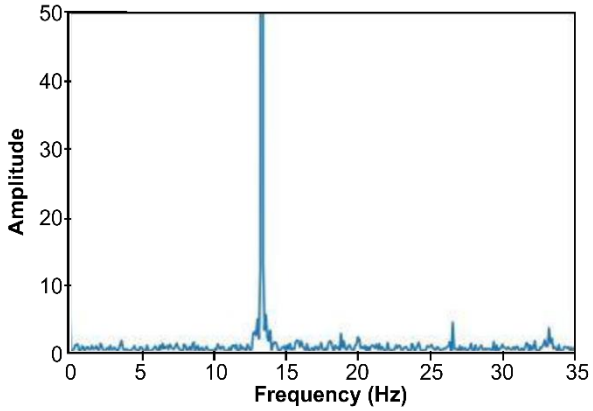


(a)

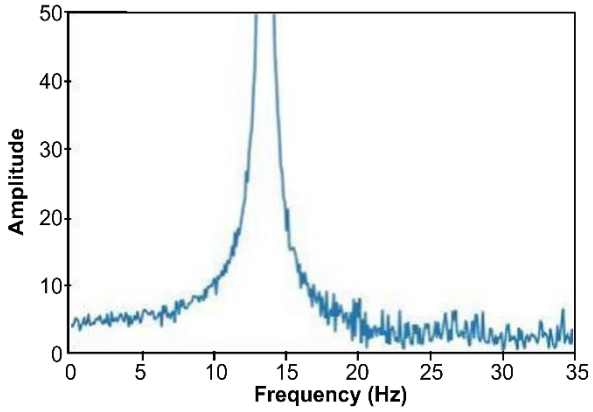


(b)

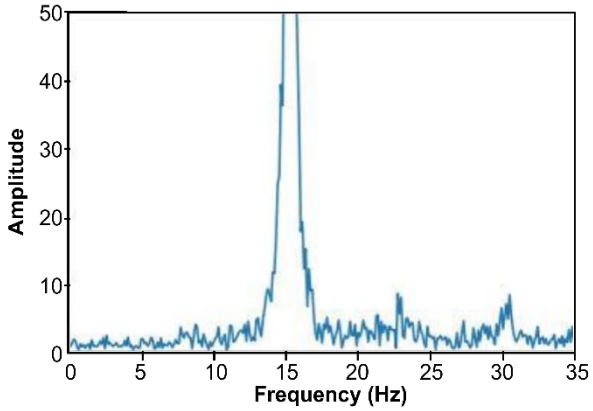


(c)

Fig. 9. FFT signal of coupling condition: (a) normal (b) 1 cm-parallel misalignment (c) 2 cm-parallel misalignment

The outcomes of signal processing can also be depicted in the frequency domain as the output resulting from the implementation of FFT. Figure 9a demonstrates the FFT signal for the normal coupling condition. It is evident that the peak frequency signal emerges at 13.5 Hz, accompanied by several minor peaks at 26.5 Hz and 34 Hz. Figure 9b displays the FFT signal for a 1 cm parallel misalignment coupling condition. The outcome of the FFT indicates multiple small peaks, including those at 14 Hz, 20 Hz, and 26.5 Hz. Figure 9c portrays the FFT signal for a 2 cm parallel misalignment coupling condition. The FFT results yield peaks at 16 Hz, 23 Hz, and 30.5 Hz.

TABLE I
CNN PROCESSING RESULT

| No | Label Data | Accuracy Result | Assessment |
|---|---|---|---|
| 1 | Normal | Normal 72.20 % | TRUE |
| 2 | Normal | Normal 68.60 % | TRUE |
| 3 | Normal | Normal 82.03 % | TRUE |
| 4 | Normal | Normal 96.59 % | TRUE |
| 5 | Normal | Normal 74.97 % | TRUE |
| 6 | Pararel | Pararel 95.40% | TRUE |
| 7 | Pararel | Pararel 99.55% | TRUE |
| 8 | Normal | Normal 82.28% | TRUE |
| 9 | Normal | Normal 71.89% | TRUE |
| 10 | Pararel | Normal 88.98% | FALSE |
| 11 | Normal | Normal 95.47% | TRUE |
| 12 | Pararel | Pararel 99.97% | TRUE |
| 13 | Normal | Normal 85.59% | TRUE |
| 14 | Pararel | Pararel 77.17% | TRUE |
| 15 | Normal | Normal 77.35% | TRUE |
| 16 | Pararel | Pararel 99.59% | TRUE |
| 17 | Pararel | Normal 86.80% | FALSE |
| 18 | Normal | Normal 73.82% | TRUE |
| 19 | Pararel | Normal 81.95% | FALSE |
| 20 | Pararel | Pararel 99.62% | TRUE |
| 21 | Pararel | Pararel 99.73% | TRUE |
| 22 | Normal | Normal 73.79% | TRUE |
| 23 | Pararel | Pararel 99.69% | TRUE |
| 24 | Normal | Normal 99.68% | TRUE |
| 25 | Pararel | Pararel 97.70% | TRUE |
| 26 | Pararel | Pararel 77.56% | TRUE |
| 27 | Normal | Normal 68.98% | TRUE |
| 28 | Pararel | Pararel 99.80% | TRUE |
| 29 | Pararel | Pararel 99.63% | TRUE |
| 30 | Pararel | Normal 80.15% | FALSE |
| 31 | Normal | Normal 83.12% | TRUE |
| 32 | Pararel | Pararel 99.88% | TRUE |
| 33 | Normal | Normal 96.04% | TRUE |
| 34 | Pararel | Pararel 97.69% | TRUE |
| 35 | Normal | Normal 89.59% | TRUE |
| 36 | Normal | Normal 91.92% | TRUE |
| 37 | Pararel | Pararel 99.37% | TRUE |
| 38 | Normal | Normal 82.81% | TRUE |
| 39 | Normal | Normal 76.41% | TRUE |
| 40 | Pararel | Pararel 99.30% | TRUE |
| 41 | Pararel | Pararel 99.81% | TRUE |
| 42 | Normal | Pararel 73.54% | FALSE |
| 43 | Pararel | Pararel 99.98% | TRUE |
| 44 | Normal | Pararel 77.06% | FALSE |
| 45 | Pararel | Normal 85.06% | FALSE |
| 46 | Normal | Normal 88.60% | FALSE |
| 47 | Pararel | Pararel 99.71% | TRUE |
| 48 | Normal | Normal 94.15% | TRUE |
| 49 | Pararel | Pararel 99.94% | TRUE |
| 50 | Normal | Normal 92.95% | TRUE |
| 51 | Pararel | Pararel 99.97% | TRUE |
| 52 | Pararel | Pararel 99.75% | TRUE |
| 53 | Pararel | Pararel 75.91% | TRUE |
| 54 | Pararel | Pararel 99.60% | TRUE |
| 55 | Pararel | Pararel 99.52% | TRUE |
| 56 | Pararel | Pararel 99.95% | TRUE |
| 57 | Normal | Pararel 76.61% | FALSE |
| 58 | Pararel | Pararel 99.99% | TRUE |
| 59 | Normal | Normal 94.09% | TRUE |
| 60 | Pararel | Pararel 99.65% | TRUE |
| 61 | Normal | Normal 84.35% | TRUE |
| 62 | Pararel | Pararel 95.58% | TRUE |
| 63 | Pararel | Normal 87.36% | FALSE |
| 64 | Normal | Normal 94.12% | TRUE |
| 65 | Normal | Normal 78.10% | TRUE |
| 66 | Normal | Normal 86.46% | TRUE |
| 67 | Normal | Normal 84.46% | TRUE |
| 68 | Normal | Normal 81.06% | TRUE |
| 69 | Normal | Pararel 77.25% | FALSE |
| 70 | Pararel | Pararel 99.39% | TRUE |
| 71 | Pararel | Pararel 99.55% | TRUE |
| 72 | Normal | Normal 82.89% | TRUE |
| 73 | Normal | Normal 96.75% | TRUE |
| 74 | Pararel | Pararel 99.82% | TRUE |
| 75 | Normal | Normal 87.63% | TRUE |
| 76 | Normal | Normal 83.34% | TRUE |
| 77 | Normal | Normal 75.86% | TRUE |
| 78 | Normal | Normal 94.40% | TRUE |
| 79 | Pararel | Pararel 77.25% | TRUE |
| 80 | Pararel | Pararel 94.59% | TRUE |

When referring to the readings from the normal condition, only a single peak at a specific frequency is visible. In this context, the FFT readings for the normal condition point to peaks at frequencies of 13.5 Hz, 26.5 Hz, and 34 Hz. In general, distinctive differences in peak frequencies exist between the 1 cm and 2 cm parallel misalignment variations. Certain peaks are absent in the normal condition, clearly indicating distinct variations in peak points between the normal and parallel conditions. Specifically, the peak for the normal condition is at 13.5 Hz, while for the 1 cm parallel misalignment, it appears at f+1fr (20 Hz), and for the 2 cm parallel misalignment, it occurs at f+1fr (23 Hz) and f+2fr (30 Hz).

### *C. Misalignment Detection using CNN*

In the process of the detection system employing CNN, a comprehensive dataset comprising 120 samples was meticulously gathered, encompassing scenarios of both standard normalcy and the parallel or abnormal state. This aggregation subsequently translated into the analysis of 240 individual data points. The dataset earmarked for the training phase constituted a substantial portion, precisely 77% or 160 samples, while the remaining 30%, equivalent to 80 samples, was dedicated to constituting the testing dataset. The outcomes of the CNN processing are meticulously documented in Table 1. Upon meticulous scrutiny of the data label, a significant distinction emerges. When the label corresponds to the state of normalcy and the reading aligns harmoniously with the same state, this congruence is acknowledged as a “TRUE” value. In contrast, if the label signifies normalcy but the actual reading suggests a state of parallel misalignment, the determination is categorized as a “FALSE” value.

The result shows that out of the 80 samples, 70 were correctly classified as true, while 10 were classified as false. Therefore, the accuracy of the CNN processing is calculated as 70/80, which equals 0.875 or 87.5%. Fig. 10 shows the graph of epoch or iteration against the accuracy of the training and testing data. A total of 100 iterations were used in the CNN model. As the number of epochs increases, the accuracy improves. In this study, the training data showed stability at epoch 60 with an accuracy of 0.87, while the testing data achieved stability at epoch 20 with an accuracy level of 0.87.

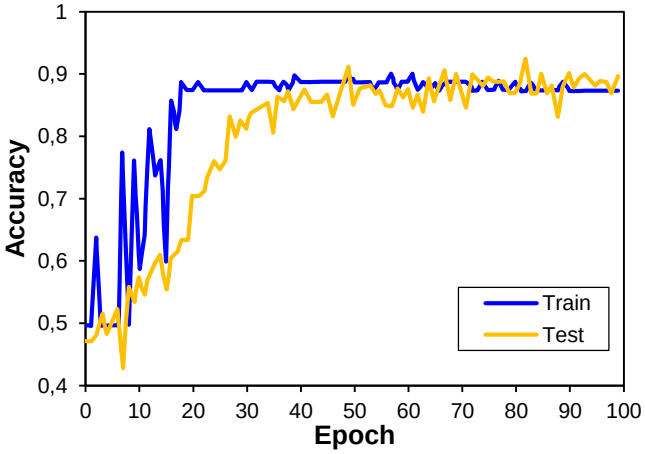


Fig. 10. Accuracy of CNN test compared to its train

## IV. CONCLUSION

The conclusions derived from this research are outlined as follows:

a. The FFT reading results for the peak in the normal condition occur at a frequency of 13.5 Hz, while for the 1 cm parallel misalignment, it emerges at f+fr (20 Hz); for the 2 cm parallel misalignment, it is situated at f+1fr (23 Hz), and f+2fr (30 Hz).
b. Through the employment of CNN, the normal and parallel conditions can be distinguished with an accuracy rate of 87.5%.

A suggestion for forthcoming research endeavors is to conduct calibration tests on the mechanical components of shaft connections.

## REFERENCES


[1] A. Pradipta, S. Triwijaya, and M. Ridwan, "Performance and Analysis of Indirect Torque Control-Based Three-Phase Induction Motor," *Elkha*, vol. 13, no. 2, p. 122, 2021.

[2] R. M. Ariefianto, R. A. Aprilianto, H. Suryoatmojo, and S. Suwito, "Design and Implementation of Z-Source Inverter by Simple Boost Control Technique for Laboratory Scale Micro-Hydro Power Plant Application," *J. Tek. Elektro*, vol. 13, no. 2, pp. 62–70, 2021.

[3] M. Appadurai, E. Fantin Irudaya Raj, and K. Venkadeshwaran, "Finite element design and thermal analysis of an induction motor used for a hydraulic pumping system," *Mater. Today Proc.*, vol. 45, pp. 7100–7106, 2021.

[4] M. R. Nuur, Y. C. Arif, and O. A. Qudsi, "Perbandingan Respon Kecepatan dan Torsi Pada Pengaturan Kecepatan Motor Induksi 3 Fasa Menggunakan Metode Vector Control dan Scalar Control," *J. EECCIS (Electrics, Electron. Commun. Control. Informatics, Syst.)*, vol. 16, no. 2, pp. 38–42, 2022.

[5] S. O. Ibrahim, K. N. Faris, and E. A. Elzahab, "Implementation of fuzzy modeling system for faults detection and diagnosis in three phase induction motor drive system," *J. Electr. Syst. Inf. Technol.*, vol. 2, no. 1, pp. 27–46, 2015.

[6] O. AlShorman, M. Irfan, N. Saad, D. Zhen, N. Haider, A. Glowacz, A. AlShorman., "A Review of Artificial Intelligence Methods for Condition Monitoring and Fault Diagnosis of Rolling Element Bearings for Induction Motor," *Shock Vib.*, vol. 2020, p. 8843759, 2020.

[7] J. D. Martínez-Morales, E. R. Palacios-Hernández, and D. U. Campos-Delgado, "Multiple-fault diagnosis in induction motors through support vector machine classification at variable operating conditions," *Electr. Eng.*, vol. 100, no. 1, pp. 59–73, 2018.

[8] B. Abouelanouar, A. Elkihel, and H. Gziri, "Experimental study on energy consumption in rotating machinery caused by misalignment," *SN Appl. Sci.*, vol. 2, no. 7, p. 1215, 2020.

[9] Z. Wang, J. Zhang, Z. Jiang, Z. Mao, K. Chang, and C. Wang, "Quantitative misalignment detection method for diesel engine based on the average of shaft vibration and shaft shape characteristics," *Measurement*, vol. 181, p. 109527, 2021.

[10] Y. Xia, J. Pang, L. Yang, Q. Zhao, and X. Yang, "Study on vibration response and orbits of misaligned rigid rotors connected by hexangular flexible coupling," *Appl. Acoust.*, vol. 155, pp. 286–296, 2019.

[11] C. Verucchi, J. Bossio, G. Bossio, and G. Acosta, "Misalignment detection in induction motors with flexible coupling by means of estimated torque analysis and MCSA," *Mech. Syst. Signal Process.*, vol. 80, pp. 570–581, 2016.

[12] J. Antonino-Daviu and P. Popaleny, "Detection of Induction Motor Coupling Unbalanced and Misalignment via Advanced Transient Current Signature Analysis," in *2018 XIII International Conference on Electrical Machines (ICEM)*, 2018, pp. 2359–2364.

[13] T. Goktas, M. Arkan, and V. Gurusamy, "A Comparative Study of Current, Vibration and Stray Magnetic Flux Based Detection for Parallel Misalignment Fault in Induction Motors," in *2021 IEEE 13th International Symposium on Diagnostics for Electrical Machines, Power Electronics and Drives (SDEMPED)*, 2021, vol. 1, pp. 11–16.

[14] S. Yu, S. Jia, and C. Xu, "Convolutional neural networks for hyperspectral image classification," *Neurocomputing*, vol. 219, pp. 88–98, 2017.

[15] J.-H. Lee, J.-H. Pack, and I.-S. Lee, "Fault Diagnosis of Induction Motor Using Convolutional Neural Network," *Applied Sciences*, vol. 9, no. 15. 2019.

[16] S. Pashaee, A. Ramezani, M. Ekresh, and S. Jorkesh, "Fault Diagnosing Of An Induction Motor Based On Signal Fusion Using One-Dimensional Convolutional Neural Network," in *2021 7th International Conference on Signal Processing and Intelligent Systems (ICSPIS)*, 2021, pp. 1–5.